NASA TECHNICAL NOTE

NASA TN D-8224

FATIGUE-CRACK INITIATION AND GROWTH IN NOTCHED 2024-T3 SPECIMENS MONITORED BY A VIDEO TAPE SYSTEM

J. A. Sova, J. H. Crews, Jr., and R. J. Exton

Langley Research Center
Hampton, Va. 23665

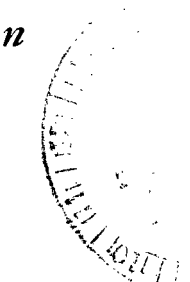

NATIONAL AERONAUTICS AND SPACE ADMINISTRATION • WASHINGTON, D. C. • AUGUST 1976

1. Report No. NASA TN D-8224	2. Government Accession No.	3. Recipient's Catalog No.
4. Title and Subtitle FATIGUE-CRACK INITIATION AND GROWTH IN NOTCHED 2024-T3 SPECIMENS MONITORED BY A VIDEO TAPE SYSTEM		5. Report Date August 1976
		6. Performing Organization Code
7. Author(s) J. A. Sova, J. H. Crews, Jr., and R. J. Exton		8. Performing Organization Report No. L-10754
		10. Work Unit No. 505-02-31-01
9. Performing Organization Name and Address NASA Langley Research Center Hampton, Va. 23665		11. Contract or Grant No.
		13. Type of Report and Period Covered Technical Note
12. Sponsoring Agency Name and Address National Aeronautics and Space Administration Washington, D.C. 20546		14. Sponsoring Agency Code

15. Supplementary Notes
J. A. Sova: NRC-NASA Research Resident Associate, now at The George Washington University, Hampton, Va.
J. H. Crews, Jr.: Langley Research Center.
R. J. Exton: Langley Research Center.

16. Abstract

Fatigue-crack initiation and early stages of growth in notched 2024-T3 aluminum alloy sheet specimens were monitored during constant-amplitude fatigue tests conducted for a range of stress ratios. A video tape system was developed to detect fatigue cracks 0.1 mm in length on the sheet surface and to monitor their growth up to a length of 1 notch radius (2.5 mm).

Fatigue cracks initiated either at the notch corner or on the notch surface. Most of the first fatigue cracks started as notch-corner cracks, and the crack-initiation period was defined as the number of cycles for which the crack was 0.1 mm in length on the sheet surface. For each of the stress ratios used, the results showed that at the low stress levels, the crack-initiation period constituted at least 90 percent of the fatigue lives. However, for the negative stress ratios at the high stress levels, cracks started as early as at about 40 percent of the fatigue lives.

For early stages of the growth of corner cracks, a linear relationship existed between the logarithm of crack length and the number of cycles. For cases of elastic cyclic stresses at the notch, experimental stress intensity factors were derived from the measured corner-crack growth rates. The factors agreed well with those calculated by several approximate analytical methods from the literature on corner-crack stress intensity factors.

17. Key Words (Suggested by Author(s)) Fatigue Propagation Initiation Circular hole Video tape system 2024-T3 aluminum alloy	18. Distribution Statement Unclassified – Unlimited Subject Category 39		
19. Security Classif. (of this report) Unclassified	20. Security Classif. (of this page) Unclassified	21. No. of Pages 31	22. Price* $3.75

*For sale by the National Technical Information Service, Springfield, Virginia 22161

FATIGUE-CRACK INITIATION AND GROWTH IN NOTCHED 2024-T3 SPECIMENS MONITORED BY A VIDEO TAPE SYSTEM

J. A. Sova,* J. H. Crews, Jr., and R. J. Exton
Langley Research Center

SUMMARY

Fatigue-crack initiation and early stages of growth in notched 2024-T3 aluminum alloy sheet specimens were monitored during constant-amplitude fatigue tests conducted for a range of stress ratios. A video tape system was developed to detect fatigue cracks 0.1 mm in length on the sheet surface and to monitor their growth up to a length of 1 notch radius (2.5 mm).

Fatigue cracks initiated either at the notch corner or on the notch surface. Most of the first fatigue cracks started as notch-corner cracks, and the crack-initiation period was defined as the number of cycles for which the crack was 0.1 mm in length on the sheet surface. For each of the stress ratios used, the results showed that at the low stress levels, the crack-initiation period constituted at least 90 percent of the fatigue lives. However, for the negative stress ratios at the high stress levels, cracks started as early as at about 40 percent of the fatigue lives.

For early stages of the growth of corner cracks, a linear relationship existed between the logarithm of crack length and the number of cycles. For cases of elastic cyclic stresses at the notch, experimental stress intensity factors were derived from the measured corner-crack growth rates. The factors agreed well with those calculated by several approximate analytical methods from the literature on corner-crack stress intensity factors.

INTRODUCTION

Aircraft structures contain stress concentration sites such as fastener and access holes. The fatigue life of these structures can be divided into three periods: the period of crack initiation at the stress concentration, the period of early crack growth near the stress concentration, and the period of crack growth away from the stress concentration. The crack growth away from the stress concentration has been studied extensively. Very

---

*NRC-NASA Research Resident Associate, now at The George Washington University, Hampton, Va.

few data, however, exist for the crack-initiation and early growth periods even though these periods can account for a large percentage of fatigue life (refs. 1 and 2). The need for more information on early crack growth has recently increased because the United States Air Force adopted airplane damage tolerance requirements that emphasize small cracks at holes (ref. 3).

The objectives of this paper are to present results of a study of the initiation and early growth of cracks at a hole and to describe a video tape monitoring system developed for this study. The case investigated was that of a 2024-T3 aluminum alloy sheet specimen containing a circular hole (also referred to as a notch in this paper).

The specimens were subjected to constant-amplitude loading at four stress ratios (R = 0.5, 0, -0.5, and -1). The applied stress levels were selected to obtain fatigue lives from about 5×10^3 cycles to about 10^7 cycles. The crack-initiation period was defined as the number of cycles for which the first fatigue crack was 0.1 mm long. Crack growth was monitored for crack lengths up to 1 hole radius (2.5 mm). When cyclic stresses at the notch were elastic, experimental stress intensity factors were derived from measured corner-crack growth rates. The factors compared favorably with those calculated by several approximate methods from the literature on corner-crack stress intensity factors.

SYMBOLS

Although values are given in SI Units in this report, some of the experimental procedures were carried out using U.S. Customary Units.

A	constant in equation relating crack length and cycles, m
a	depth of corner crack, m
B	coefficient in equation (2) relating logarithm of crack length to cycles, 1/cycle
C_1	constant in equation for fatigue-crack growth
c	crack length on the specimen surface measured from edge of hole, m
c_e	effective crack length, m
D	hole diameter, m
f_1	stress intensity correction factor to account for effect of hole on semielliptical crack

f_b	stress intensity correction factor to account for the effect of hole on through crack
f_w	finite width correction factor for stress intensity
K	stress intensity factor, $MN/m^{3/2}$
K_{max}	stress intensity factor corresponding to S_{max}, $MN/m^{3/2}$
M_1	front surface correction factor for stress intensity
M_e	specimen boundary correction factor for stress intensity
N	number of cycles
N_c	number of cycles corresponding to crack length c
N_f	fatigue life, cycles
N_i	crack-initiation period, cycles
N_p	number of cycles after crack-initiation period
n	exponent in equation for fatigue-crack growth
p	exponent in equation for specimen-boundary correction factor
Q	crack shape factor
R	stress ratio, S_{min}/S_{max}
S_g	nominal gross-section stress, Pa
S_{max}	maximum nominal net-section stress, Pa
S_{min}	minimum nominal net-section stress, Pa
t	specimen thickness, m

w	specimen width, m
α_b	back surface correction factor for stress intensity
α_f	front surface correction factor for stress intensity
β	angle in the plane of semielliptical crack, deg
λ	dimensionless crack length factor
Φ	elliptical integral for elliptical cracks

APPARATUS AND EXPERIMENTAL PROCEDURE

Figure 1 shows the configuration of the notched specimen. When loaded uniaxially, the specimen has an elastic stress concentration factor of 2.81 (ref. 4). The specimens were made from 2.28-mm-thick sheets of 2024-T3 aluminum alloy. To reduce the residual stresses caused by machining, the holes were predrilled and then enlarged by increments of 0.5, 0.2, and 0.1 mm to arrive at the 5.0-mm diameter. Only new, high-speed drills were used. Drill speed and feed were about 700 rpm and 0.05 mm per revolution, respectively. The specimens were drilled in stacks of 3, and the drills were replaced after drilling through 10 stacks. The specimen surfaces near the hole were gently polished to deburr the hole and to facilitate the detection of cracks.

The fatigue tests were conducted in a hydraulically actuated, closed-loop, servocontrolled testing machine similar to the one described in reference 5. Constant-amplitude axial loadings were applied at four stress ratios (R = 0.5, 0, -0.5, and -1). Applied stresses were selected to obtain fatigue lives ranging from about 5×10^3 to 10^7 cycles. Cyclic frequencies in the range of 5 to 20 Hz were used. Generally, three specimens were tested for each test condition. Antibuckling guide plates were used on specimens loaded in compression. The fatigue critical points are on the transverse axis of the specimen at the edges of the hole. Therefore, during the fatigue tests, four areas (two at each side of the specimen) were simultaneously monitored for cracks.

A video tape system was developed to view the crack-initiation sites. A diagram of the system is sketched in figure 2. An overall view of the system installed at the testing machine is shown in figure 3, and a closeup view of the four television cameras viewing the specimen is shown in figure 4. The images of the four crack-initiation sites were magnified and fed to a special effects (quad-split) generator which combined the four outputs into a single simultaneous four-quadrant picture. This composite picture was then

fed to a video counter which electronically superimposed the accumulated number of cycles onto the four-quadrant view. Finally the picture was recorded on video tape for later analysis and was also fed to a monitor for real-time viewing. The magnification of the system was ×60. During testing, the specimen was illuminated by strobe lamps which were synchronized to the fatigue machine. The strobe lamps were triggered at the point of maximum load of each cycle when cracks were open and most visible. A view of cracks as they appeared on the monitor is shown in figure 5. The video tape system is described in more detail in appendix A.

CRACK-INITIATION AND GROWTH RESULTS

Crack Initiation

After each fatigue test, a scanning electron microscope was used to locate the crack-initiation sites on the fracture surface. The cracks initiated in the two ways shown in figure 6 and are referred to in this study as notch-corner cracks and notch-surface cracks. In about 75 percent of the tests, the first cracks started at a notch corner, and their initiation and growth were readily observed on the sheet surfaces by the television cameras. In the remaining tests, the first cracks started on the notch surface and their initial growth was not observed. Notch-surface cracks were observed only after they had penetrated to the sheet surface and, as a result, are not included in the following discussion of crack initiation.

The crack-initiation period was defined as the number of cycles for which the first notch-corner crack was 0.1 mm long on the sheet surface. The results are presented in table I and figure 7. Figure 7 presents fatigue lives (complete failure of specimens) and crack-initiation periods for the four stress ratios investigated. The symbols represent the average numbers of cycles obtained for each test condition. In general, the initiation curves have the same shape as the failure curves. The trends in these data are shown more conveniently in figure 8 where crack-initiation periods are plotted as percentages of fatigue lives. For the range of fatigue lives investigated, the length of the crack-initiation period depends on both the stress ratio R and the applied maximum stress S_{max}. For $R = 0.5$ and 0, the crack-initiation periods constituted more than about 70 percent of the fatigue lives. For $R = -0.5$ and -1, some fatigue cracks started as early as at about 40 percent of the fatigue lives. However, for all the R-ratios tested, the results obtained for low applied stresses (corresponding to lives longer than 10^6 cycles) showed that the crack-initiation periods covered at least 90 percent of the fatigue lives. The shapes of the crack-initiation curves (fig. 8) are discussed at greater length in the following section.

An overall analysis of the notch-corner-crack results in table I indicates that the scatter in fatigue lives obtained for a particular stress level was mainly the result of

scatter in crack initiation. Also, a comparison of results for specimens with notch-corner cracks and for those with notch-surface cracks shows no obvious influence of the crack type on the fatigue life. The notch-surface cracks were more likely to occur for stress ratios $R = 0.5$ and 0, particularly at high applied stresses.

Crack Growth

A typical plot of crack growth is shown in figure 9 for $R = -0.5$ and $S_{max} = 150$ MPa. Note that crack length c (on the sheet surface) is presented on a logarithmic scale and the number of cycles is on a linear scale. The four crack growth curves start from points labeled A, B, C, and D. These points correspond to the four corners of the notch. The first observed crack initiated as a notch-corner crack at point A. During the initial stage of growth, a linear relationship existed between the logarithm of the crack length and the number of cycles. The extent of the linear relationship and its slope are presented in table I. The crack grew through the thickness approximately in the manner shown in figure 9. At the time of penetration to B, the crack length AE on the sheet surface was less than the specimen thickness. The crack grew very rapidly from B until BG = AF. The second crack CD initiated on the notch surface late in the fatigue life and grew rapidly after it reached the sheet surfaces. Second cracks typically initiated in this way and are excluded from subsequent discussion.

The first crack initiated on the notch surface in about 25 percent of the fatigue tests. A comparison of typical results for notch-surface and notch-corner cracks is presented in figure 10 for two replicate tests at $R = 0$ and $S_{max} = 200$ MPa. For the test results presented at the right of the figure, the first crack initiated at the notch corner and in this semilog plot grew linearly from point A. In the other test, the first crack initiated on the notch surface and could not be observed by the cameras until it had penetrated to the sheet surface at point A. The subsequent crack growth on the sheet surface was rapid and nonlinear; however, the crack assumed the rate of the notch-corner crack when the crack configuration matched that of a corner crack. (See point P, fig. 10.) Although in the tests presented in figure 10 the notch-surface crack initiated earlier than the notch-corner crack, no systematic trend of this type was found in this investigation.

Table I gives the crack lengths on one specimen surface at the time the crack penetrated the sheet to the other surface. The lengths of these notch-corner cracks vary from 40 percent to 83 percent of the specimen thickness, depending on applied stress. The crack lengths of notch-surface cracks at the time of penetration are shorter than those of notch-corner cracks; the lengths of the cracks also depend on where the crack started. For example, a crack that initiated in midthickness would appear simultaneously on both sheet surfaces. In several tests, the fractographic examination indicated that a notch-surface crack probably initiated while a crack growth was being recorded on the sheet surface. Results for such cases are labeled in table I.

Table I also gives the cycles corresponding to various first-crack lengths up to 1 hole radius (2.5 mm). These cycles are plotted in figure 11 as percentages of fatigue lives for the various corner-crack lengths. (Curves for $c = 0.1$ mm in fig. 11 also appeared earlier in fig. 8.) The results show that in most cases, more than 90 percent of fatigue life is required to produce a crack 1 hole radius long (2.5 mm).

Most of the curves in figure 11 show a minimum percent of fatigue life required to grow a crack to a particular size. Several studies have shown that the trend is toward large percentages at low stresses. (See, for example, refs. 1 and 2.) However, above the minimum, the trend for larger percentages at high stresses was not expected. This trend can be explained by the consideration of an extreme case in which the maximum stress is large enough to fail the cracked specimen when the crack grows to a length of only 0.1 mm. This maximum stress would be near the ultimate strength of the material, and 100 percent of the fatigue life would be required to grow the crack to 0.1 mm. Therefore, the curves for $c = 0.1$ mm in figure 11 should approach an upper extreme point defined by $N_c/N_f = 100$ percent and S_{max} nearly equal to the ultimate strength of the material (about 500 MPa). Similarly, other curves in figure 11 should each approach an upper extreme at $N_c/N_f = 100$ percent and S_{max} equal to the failure strength for each particular crack size. Although these extremes were not established, the trends in figure 11 agree with this interpretation of the results.

ANALYSIS OF CORNER-CRACK GROWTH MEASUREMENTS

The observed linear relationship between $\log c$ and cycles was analyzed in terms of stress intensity factors for a small corner crack at a circular hole. Experimental stress intensity factors were derived from measured crack growth rates and were then compared with approximate stress intensity factors from the literature.

Several investigators have used measured crack growth rates to calculate stress intensity factors. (See, for example, ref. 6.) Such calculations were based on an equation relating crack growth rate to stress intensity factor for a constant R-ratio (ref. 7). The equation, in the notation of this paper, is

$$\frac{dc}{dN} = C_1\left(K_{max}\right)^n \tag{1}$$

In equation (1), K_{max} is used instead of the usual range of stress intensity ΔK because, as explained later, only cases with negative R are analyzed; the compressive portion of the loading cycle is neglected here in calculating stress intensity factors as it was in reference 8. The constants C_1 and n are established by crack growth tests involving

known stress intensity factors. Then, measured dc/dN values for a complex case can be substituted into equation (1) to find the corresponding K_{max} values.

In the present study, the measured linear portions of the crack growth curves could be represented by

$$\log c = A + BN_p \tag{2}$$

where N_p is the number of loading cycles after crack initiation. Because crack initiation was defined by $c = 0.1$ mm, A was equal to $\log (0.1)$. The slope B was determined from the linear portion of the crack growth curve (plotted as c on a logarithmic scale against N on a linear scale). Differentiation of equation (2) leads to

$$\frac{dc}{dN} = 2.3Bc \tag{3}$$

Substitution of equation (3) into equation (1) results in an equation for stress intensity:

$$K_{max} = \left(\frac{2.3Bc}{C_1}\right)^{1/n} \tag{4}$$

In this study, equation (4) could be applied to only two test cases: $S_{max} = 100$ MPa with $R = -1$ and $S_{max} = 125$ MPa with $R = -0.5$. For all other cases, yielding either altered the local stress ratio R or it caused cyclic plasticity near the hole. (See, for example, ref. 9.) Neither of these effects was accounted for by the present procedure.

For the case where $S_{max} = 100$ MPa with $R = -1$, the constants n and C_1 were obtained from $R = -1$ crack growth data for center-cracked sheets in reference 8 and were, respectively, 3.39×10^{-11} and 3.79×10^{-11} (with dc/dN expressed in m/cycle and K_{max} in $MN/m^{3/2}$). These two constants and the extreme values of B for this test case (see table I) were substituted into equation (4) to obtain the corresponding "scatter band" for the experimental K_{max}. These results are shown as the shaded region in figure 12(a). For purposes of comparison, figure 12(a) also shows several approximate stress intensity solutions for corner cracks from the literature. (See appendix B.) Most of the solutions agree closely with the experimental K_{max} of this study for the range $0.02 \leqq c/D \leqq 0.2$. This range corresponds to $0.1 \text{ mm} \leqq c \leqq 1.0$ mm. However, the trends in figure 12(a) show that the approximate solutions would not agree closely with an extrapolation of the experimental results. Consequently, caution should be exercised in extrapolating the linear-growth curves observed in this study.

Although the crack growth data for the $R = -0.5$ case were not available in the literature, data were available (ref. 8) for $R = 0$ and $R = -1$ which bracket this case. Approximate values of n and C_1 for $R = -0.5$ were obtained from the $R = 0$ and $R = -1$ data by averaging the stress intensity factors for given crack growth rates. (Since the $R = 0$ and $R = -1$ curves in ref. 8 differed by only about 20 percent, this procedure introduced errors that were no larger than about ±10 percent.) The experimental K_{max} values for the case where $S_{max} = 125$ MPa with $R = -0.5$ are represented in figure 12(b) by the shaded zone. The experimental K_{max} and the approximate solutions agreed reasonably well for the range $0.02 \leqq c/D \leqq 0.2$.

CONCLUDING REMARKS

A video tape system was developed to monitor the growth of small fatigue cracks. The system was used to record the growth of small cracks in center-hole (theoretical elastic stress concentration factor of 2.81) 2024-T3 aluminum alloy specimens for constant-amplitude loadings at four stress ratios (0.5, 0, -0.5, and -1). From this investigation the following were concluded:

1. The video tape system detected fatigue cracks 0.1 mm in length and monitored their growth up to 1 notch radius (2.5 mm).

2. Fatigue cracks initiated either at the corner formed by specimen and hole surfaces (notch-corner cracks) or on the hole surface (notch-surface cracks). In about 75 percent of the fatigue tests, first cracks started as notch-corner cracks. The type of crack to initiate first had no obvious influence on the fatigue lives.

3. The number of cycles for which a notch-corner crack was 0.1 mm long was defined at the crack-initiation period. For the range of fatigue lives investigated, the percentage of fatigue life spent in crack initiation depended on both the stress ratio and the applied maximum stress. For stress ratios of 0.5 and 0, the crack-initiation periods accounted for more than about 70 percent of the fatigue lives. For high applied stresses with stress ratios of -0.5 and -1, fatigue cracks started as early as at about 40 percent of the fatigue lives. However, for any stress ratio and low applied stresses (corresponding to lives longer than 10^6 cycles) cracks started after at least 90 percent of the fatigue lives.

4. The crack growth results showed that for most tests, more than 90 percent of fatigue life was required to produce a crack 1 hole radius long (2.5 mm).

5. For the growth of very small notch-corner cracks, a linear relationship existed between the logarithm of crack length and the number of cycles.

6. Experimental stress intensity factors were derived from measured corner-crack growth rates for two stress levels at which the local stresses at the hole were elastic

(stress ratio of -1, maximum stress of 100 MPa and stress ratio of -0.5, and maximum stress of 125 MPa). For ratios of crack length to hole diameter between 0.02 and 0.2, the experimental factors agreed reasonably well with those calculated by several approximate analytical methods from the literature.

Langley Research Center
National Aeronautics and Space Administration
Hampton, Va. 23665
May 27, 1976

APPENDIX A

VIDEO TAPE CRACK DETECTION SYSTEM

General Description

The video tape monitoring system employed four TV cameras to view the crack-initiation sites at the notch. A diagram of the system is shown in figure 2, and an overall view of the system installed at the fatigue machine is shown in figure 3. The specimen was illuminated by strobe lamps which were synchronized to the fatigue machine. The strobe lamps were triggered at the point of maximum stress of each cycle, when cracks were open and most visible. The lamps had a pulse duration of approximately 1 μs which provided effective stop-action viewing of the specimen. The outputs from the four cameras were fed to a special effects (quad-split) generator which combined the four outputs into a single simultaneous four-quadrant view. This composite view was then fed to a video counter which electronically superimposed the accumulated number of cycles onto the quadrant view. Finally, the composite video signal was fed to a video tape recorder to be stored for later analysis and to a monitor for real-time viewing.

Vidicon Tubes

The vidicon tubes in the TV cameras had to be specially constructed because the 1-μs duration of the strobe lamps presented a special problem for the system. A standard TV system has a field rate of 60 fields per second (16.7 ms per field), and a standard vidicon tube has a persistence time of about 15 ms. (Persistence time (lag time) is time required for video signal to fall to one-half of its original value.) A fatigue machine operating at 20 Hz would, therefore, generate one pulse of the strobe lamps every 50 ms. The result would be one bright field in which the flash occurs, followed by several fields in which there is no illumination. An image flicker would thereby be generated which was unsuitable for data analysis. The solution to this problem was to increase the persistence time of the vidicon tubes. The tubes selected had a 250 ms persistence time. The stop-action image produced by a given flash was retained for many field scans, thus eliminating flicker. However, this flicker-free operation was gained at the expense of time resolution, but the loss of time resolution was not significant for the present study which dealt only with slow crack growth rates. For example, the 250 ms persistence time corresponds to 5 cycles of the fatigue machine at 20 Hz and 1.25 cycles at 5 Hz.

Magnification and Resolution

Magnification was achieved through combined optical and electronic magnifications. The cameras had f/1.9 lenses with a focal length of 75-mm and 100-mm extenders which

resulted in an optical magnification of about ×1.5. An electronic magnification of ×40 was attained in going from the vidicon tube to the monitor screen. The overall magnification was, therefore, ×60.

Higher magnification could have been obtained optically, but the compromise here between resolution and field size was chosen so that small cracks could be detected and monitored until they reached a length of 1 hole radius (2.5 mm). To enhance crack detection, each camera was mounted on its side so that cracks would extend across the scan lines, rather than run parallel to them. Crack lengths of 0.1 mm were measured routinely while the smallest perceptible crack length was about 0.05 mm.

Counter and Recorder

The quad-split generator received four video inputs and displayed a portion of each in the composite quadrant view. Thin margins separated the four views. The size of an individual view was apportioned by translating the vertical and horizontal margins. The composite picture generated in the quad-split generator was sent to a video counter which superimposed a digital display. This display included four digits for test identification (test number) and seven digits for recording the accumulated number of loading cycles.

The quadrant view and superimposed digital display were recorded by a 1-inch video tape recorder capable of $3\frac{1}{2}$ hours of continuous recording. At the end of this period, the tape was rewound, when necessary, and recording was continued; earlier data were thus erased from the tape. This procedure was repeated until specimen failure, after which replay of the tape allowed crack growth to be traced backward to the time of crack initiation.

Illumination and Data Reading

The illumination selected for this study resulted in the observation of "white" cracks against a black background. Two strobe lamps (one at each side of the specimen) were located out of the plane of the crack and cameras. Very little light was diffusely reflected toward the lens from the smooth surface although small surface scratches did cause some reflection. When the crack appeared, more light was scattered toward the camera. This added light produced a white crack against a black background.

After each test, the tape was replayed to determine the number of loading cycles corresponding to crack initiation. A scale was attached to the monitor near the crack growth path, and the numbers of cycles were copied for several crack lengths as the video tape was replayed. A typical display is shown in figure 5.

APPENDIX B

APPROXIMATE STRESS INTENSITY FACTORS

Although an exact solution for a corner crack at a circular hole has not been developed, approximate solutions exist. Five such solutions are presented here for comparison with the experimental stress intensity factors found in the present study.

1. In reference 10, Newman developed the following approximate solution for a single corner crack at a circular hole by superimposing a crack shape factor, boundary correction factors, and the Bowie correction for the hole:

$$K = S_g\sqrt{\pi \frac{a}{Q}}\, M_e \sqrt{\sec\left(\frac{\pi D}{2w}\right)}\, f_b(c,D) \tag{B1}$$

The crack shape factor Q was expressed as

$$Q = 1 + 1.47\left(\frac{a}{c}\right)^{1.64}$$

The specimen-boundary correction factor M_e was given as

$$M_e = \left[M_1 + \left(\sqrt{Q\,\frac{c}{a}} - M_1\right)\left(\frac{a}{t}\right)^p\right] f_w$$

where the front surface correction factor M_1 was

$$M_1 = 1.2 - 0.1\left(\frac{a}{c}\right)$$

and

$$p = 2 + 8\left(\frac{a}{c}\right)^3$$

The finite width correction factor f_w was

$$f_w = \sqrt{\sec\left[\frac{\pi}{2}\left(\frac{D + c}{w - c}\right)\sqrt{\frac{a}{t}}\right]}$$

APPENDIX B

The Bowie correction f_b (ref. 11) was approximated by

$$f_b = 0.707 - 0.18\lambda + 6.55\lambda^2 - 10.54\lambda^3 + 6.85\lambda^4$$

where

$$\lambda = \left(1 + \frac{2c}{D}\right)^{-1}$$

2. Shah developed a solution in reference 12 for two elliptical cracks symmetrically located at a circular hole. He then introduced surface correction factors and a single corner-crack correction to get

$$K = \alpha_f \alpha_b \frac{S_g}{\Phi}\sqrt{\pi a}\left[\cos^2\beta + \left(\frac{a}{c}\right)^2 \sin^2\beta\right]^{1/4}\sqrt{\frac{D + \pi\frac{ac}{4t}}{D + 2\pi\frac{ac}{4t}}}\, f_1 \qquad \text{(B2)}$$

where Φ is the well-known elliptical integral applicable to elliptical cracks. The α_f and α_b are front and back surface correction factors, respectively. For the present study, $\alpha_f = 1.11$, $\alpha_b = 1$, and $\beta = 90^\circ$. The function f_1 is given in graphical form in reference 12.

3. Hall and Finger (ref. 13) derived the following empirical expression from fracture data for specimens with corner cracks at holes

$$K = 0.87 S_g \sqrt{\pi c_e}\, f_b(c_e, D) \qquad \text{(B3)}$$

The c_e represents an effective crack size which was presented as an empirical curve in reference 13. Note that the Bowie correction f_b is evaluated for c_e.

4. Liu (ref. 14) also developed an approximate solution in terms of an effective crack size, but he used it only in the Bowie correction factor

$$K = \alpha_b \alpha_f \frac{S_g}{\Phi}\sqrt{\pi c}\, f_b(c_e, D) \qquad \text{(B4)}$$

where

$$c_e = \frac{1}{2}\sqrt{2}\, c$$

Liu took $\alpha_f = 1.12$ and for the present study $\alpha_b = 1$.

5. Smith (ref. 15) used the standard elliptical crack solution and applied the Bowie correction factor to develop an approximate corner-crack solution:

$$K = \frac{S_g}{\Phi}\sqrt{\pi \frac{a^2}{c}}\, f_b(c,D) \tag{B5}$$

REFERENCES

1. Schijve, J.; and Jacobs, F. A.: Fatigue Crack Propagation in Unnotched and Notched Aluminum Alloy Specimens. NLR-TR M.2128, Nat. Aero-Astronaut. Res. Inst. (Amsterdam), May 1964.

2. Sova, J. A.; and Williams, T. R. G.: Fatigue Properties of the Alclad Al-Cu-Mg-Si-Mn Alloy. Aeronaut. J. Roy. Aeronaut. Soc., vol. 78, no. 764, Aug. 1974, pp. 375-379.

3. Military Specification. Airplane Damage Tolerance Requirements. MIL-A-83444 (USAF), July 2, 1974.

4. Howland, R. C. J.: On the Stresses in the Neighbourhood of a Circular Hole in a Strip Under Tension. Phil. Trans. Roy. Soc. (London), ser. A, vol. 229, no. 671, Jan. 6, 1930, pp. 49-86.

5. Imig, L. A.: Effect of Initial Loads and of Moderately Elevated Temperature on the Room-Temperature Fatigue Life of Ti-8Al-1Mo-1V Titanium-Alloy Sheet. NASA TN D-4061, 1967.

6. Grandt, A. F., Jr.; and Hinnerichs, T. D.: Stress Intensity Factor Measurements for Flawed Fastener Holes. Proceedings of Army Symposium on Solid Mechanics; The Role of Mechanics in Design – Structural Joints. AMMRC MS 74-8, U.S. Army Material Command, Sept. 1974, pp. 161-176. (Available from DDC as AD-786 543.)

7. Paris, Paul C.; Gomez, Mario P.; and Anderson, William E.: A Rational Analytic Theory of Fatigue. Trend Eng. (Univ. of Washington), vol. 13, no. 1, Jan. 1961, pp. 9-14.

8. Hudson, C. Michael: Effect of Stress Ratio on Fatigue-Crack Growth in 7075-T6 and 2024-T3 Aluminum-Alloy Specimens. NASA TN D-5390, 1969.

9. Crews, John H., Jr.: Elastoplastic Stress-Strain Behavior at Notch Roots in Sheet Specimens Under Constant-Amplitude Loading. NASA TN D-5253, 1969.

10. Newman, J. C., Jr.: Predicting Failure of Specimens With Either Surface Cracks or Corner Cracks at Holes. NASA TN D-8244, 1976.

11. Bowie, O. L.: Analysis of an Infinite Plate Containing Radial Cracks Originating at the Boundary of an Internal Circular Hole. J. Math. & Phys., vol. XXXV, no. 1, Apr. 1956, pp. 60-71.

12. Shah, R. C.: Stress Intensity Factors for Through and Part-Through Cracks Originating at Fastener Holes. Mechanics of Crack Growth, ASTM Spec. Tech. Publ. 590, c.1976, pp. 429-459.

13. Hall, L. R.; and Finger, R. W.: Fracture and Fatigue Growth of Partially Embedded Flaws. Proceedings of the Air Force Conference on Fatigue and Fracture of Aircraft Structures and Materials, H. A. Wood, R. M. Bader, W. J. Trapp, R. F. Hoener, and R. C. Donat, eds., AFFDL-TR-70-144, U.S. Air Force, Dec. 1970, pp. 235-262. (Available from DDC as AD 719 756.)

14. Liu, A. F.: Stress Intensity Factor for a Corner Flaw. Eng. Fracture Mech., vol. 4, no. 1, Mar. 1972, pp. 175-179.

15. Smith, Samuel H.: Fatigue-Crack Growth Behavior of C-5A Wing Control Points. ASD-TR-74-18, U.S. Air Force, May 1974. (Available from DDC as AD-A002 553.)

TABLE I.- CRACK INITIATION AND GROWTH DATA FOR NOTCHED 2024-T3 ALUMINUM ALLOY SPECIMENS

Stress ratio, R	Stress, S_{max}, MPa	Type of first crack, C for corner and S for surface	Fatigue life, N_f, cycles	Cycles to crack length (c) of . . ., mm					Extent of linear relationship, mm	Coefficient in eq. (2), B, 1/cycle	Length of crack at penetration through sheet, c, mm
				0.1 (initiation)	0.2	0.5	1.0	2.5			
0.5	400	[a]S	4 860	4 810	4 828	4 852	(b)	(b)	----	----------	0.11
		[a]C	7 840	6 380	6 975	7 380	7 630	(b)	[c]0.25	5.06×10^{-4}	[c].50
		[a]C	8 810	6 780	7 335	8 055	8 560	(b)	[c].80	5.48×10^{-4}	[c]1.30
	350	C	22 780	17 450	18 370	19 630	20 640	22 300	0.85	3.21×10^{-4}	0.90
		[a]C	24 550	19 500	20 250	21 240	22 000	23 550	[c]1.20	4.00×10^{-4}	[c].70
		S	27 110	24 680	24 750	25 060	25 640	26 750	----	----------	.44
	250	S	91 700	65 600	65 940	66 570	68 250	73 600	----	----------	0.40
		C	132 780	107 200	112 000	118 350	123 200	128 500	1.30	6.25×10^{-5}	1.70
		C	4 846 300	4 802 500	4 808 200	4 815 600	4 821 300	4 828 700	>2.5	5.33×10^{-5}	1.50
	225	---	>10 000 000	--------	--------	--------	--------	--------	----	----------	----
0	350	C	3 810	2 740	2 990	3 315	3 560	3 790	1.40	1.22×10^{-3}	1.10
		S	4 140	3 370	3 456	3 635	3 835	4 080	----	----------	.20
		[a]C	4 920	3 645	3 935	4 320	4 610	4 860	[c]1.30	1.04×10^{-3}	[c]1.00
	250	C	22 550	15 300	17 000	19 220	20 600	21 700	0.80	1.78×10^{-4}	1.35
		S	22 620	18 550	18 700	19 050	19 730	21 150	----	----------	.62
		S	34 420	24 600	26 050	27 950	30 700	32 900	----	----------	1.05
	200	S	76 260	54 100	54 200	56 200	59 500	64 700	----	----------	1.40
		C	110 840	91 400	95 100	100 100	103 800	107 200	1.00	8.06×10^{-5}	1.25
		C	115 760	90 200	93 580	98 200	101 800	106 400	>2.50	8.63×10^{-5}	1.70
	150	S	329 000	285 300	285 600	286 000	286 500	293 600	----	----------	0.30
		C	5 270 900	5 193 400	5 200 800	5 210 500	5 218 000	5 227 800	>2.50	4.06×10^{-5}	1.60
		C	5 423 900	5 369 400	5 374 000	5 379 800	5 384 500	5 394 000	1.35	6.62×10^{-5}	1.35

[a]Notch-surface crack initiated while crack growth was being recorded on the sheet surface.

[b]Specimen failed before crack reached that length.

[c]Numbers are not typical of corner cracks because crack growth was altered by notch-surface crack (see footnote a).

[d]Data lost because equipment failed.

TABLE I.- Concluded

Stress ratio, R	Stress, S_{max}, MPa	Type of first crack, C for corner and S for surface	Fatigue life, N_f, cycles	Cycles to crack length (c) of . . ., mm					Extent of linear relationship, mm	Coefficient in eq. (2), B, 1/cycle	Length of crack at penetration through sheet, c, mm
				0.1	0.2	0.5	1.0	2.5			
-0.5	250	S	4 610	3 080	3 180	3 590	3 915	4 340	-----	----------	1.40
		[a]C	5 760	2 720	3 945	4 500	4 910	5 400	[c]0.20	2.46×10^{-4}	[c].42
		[a]C	6 280	2 680	3 800	4 660	5 080	5 640	[c].27	2.69×10^{-4}	[c].20
	200	C	24 600	9 000	12 550	17 300	19 800	22 200	0.58	8.42×10^{-5}	1.45
		C	27 160	14 000	16 920	20 750	22 800	25 300	.50	1.03×10^{-4}	1.60
		C	33 260	14 600	18 500	26 000	29 200	31 000	.40	7.72×10^{-5}	1.30
	150	S	127 180	98 800	99 200	99 800	100 850	106 300	-----	----------	0.43
		C	169 160	125 250	130 200	136 800	141 800	148 400	>2.50	6.04×10^{-5}	1.80
		C	543 080	480 000	491 200	506 000	512 200	519 400	.50	2.69×10^{-5}	1.70
	125	C	1 557 700	1 452 000	1 469 400	1 492 500	1 510 000	1 523 700	1.00	1.72×10^{-5}	1.88
		C	1 753 700	1 652 700	1 668 000	1 688 300	1 701 300	1 712 500	.80	1.96×10^{-5}	1.70
		C	2 327 540	2 208 000	2 228 600	2 256 600	2 277 800	2 293 000	1.10	1.43×10^{-5}	1.80
-1.0	200	[a]C	6 260	2 000	2 800	3 860	4 520	5 260	[c]0.66	3.76×10^{-4}	[c]0.42
		[a]C	6 400	3 000	3 600	4 400	5 000	5 800	[c]>2.50	5.00×10^{-4}	[c].90
		[a]C	6 680	2 400	3 320	4 750	5 270	5 960	[c].22	3.27×10^{-4}	[c].86
	150	C	40 320	14 000	17 850	22 900	26 820	32 000	>2.50	7.80×10^{-5}	1.45
		S	58 280	41 400	41 820	42 500	43 200	46 800	-----	----------	.43
		C	70 990	46 800	50 850	56 300	60 400	65 800	>2.50	7.35×10^{-5}	1.80
	100	C	1 586 200	1 426 000	1 447 700	1 476 600	1 498 000	1 519 000	1.25	1.39×10^{-5}	1.90
		C	1 681 000	1 480 000	1 512 500	1 556 000	1 588 700	1 605 500	1.00	9.20×10^{-6}	1.60
		C	2 481 290	2 343 000	2 371 400	(d)	(d)	(d)	(d)	1.06×10^{-5}	(d)

[a]Notch-surface crack initiated while crack growth was being recorded on the sheet surface.

[b]Specimen failed before crack reached that length.

[c]Numbers are not typical of corner cracks because crack growth was altered by notch-surface crack (see footnote a).

[d]Data lost because equipment failed.

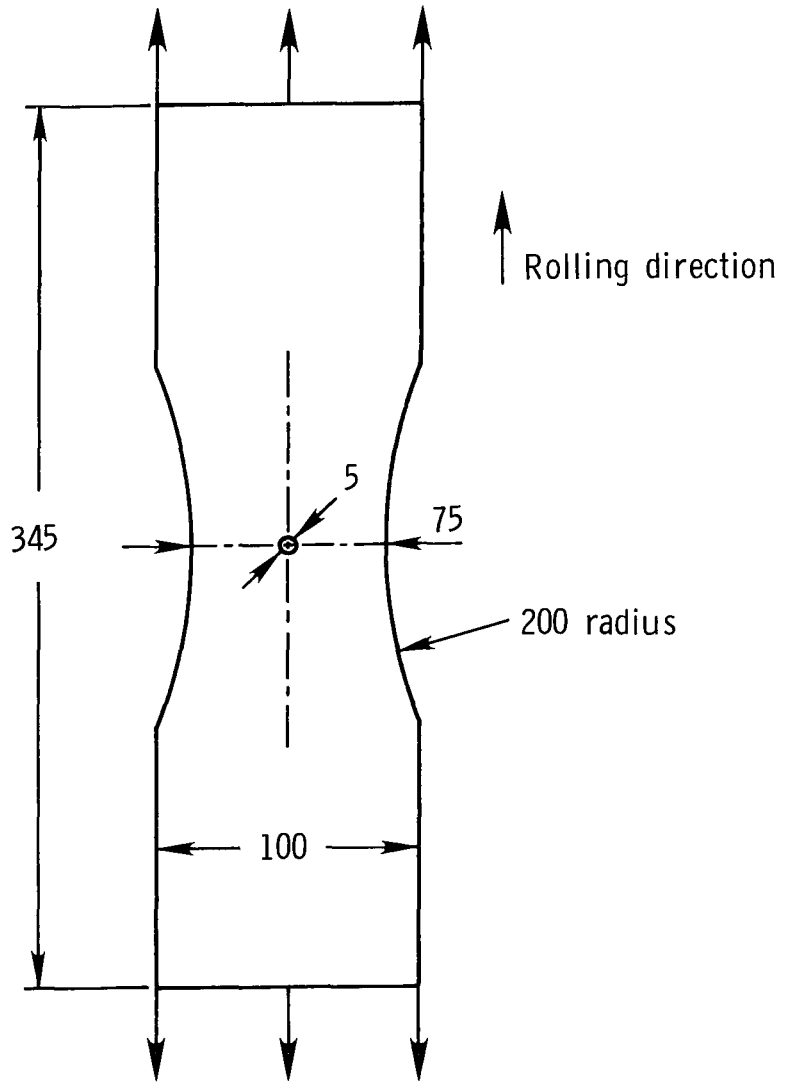

Figure 1.- Fatigue specimen. Material: 2024-T3 aluminum alloy; thickness, 2.28 mm. All dimensions in mm.

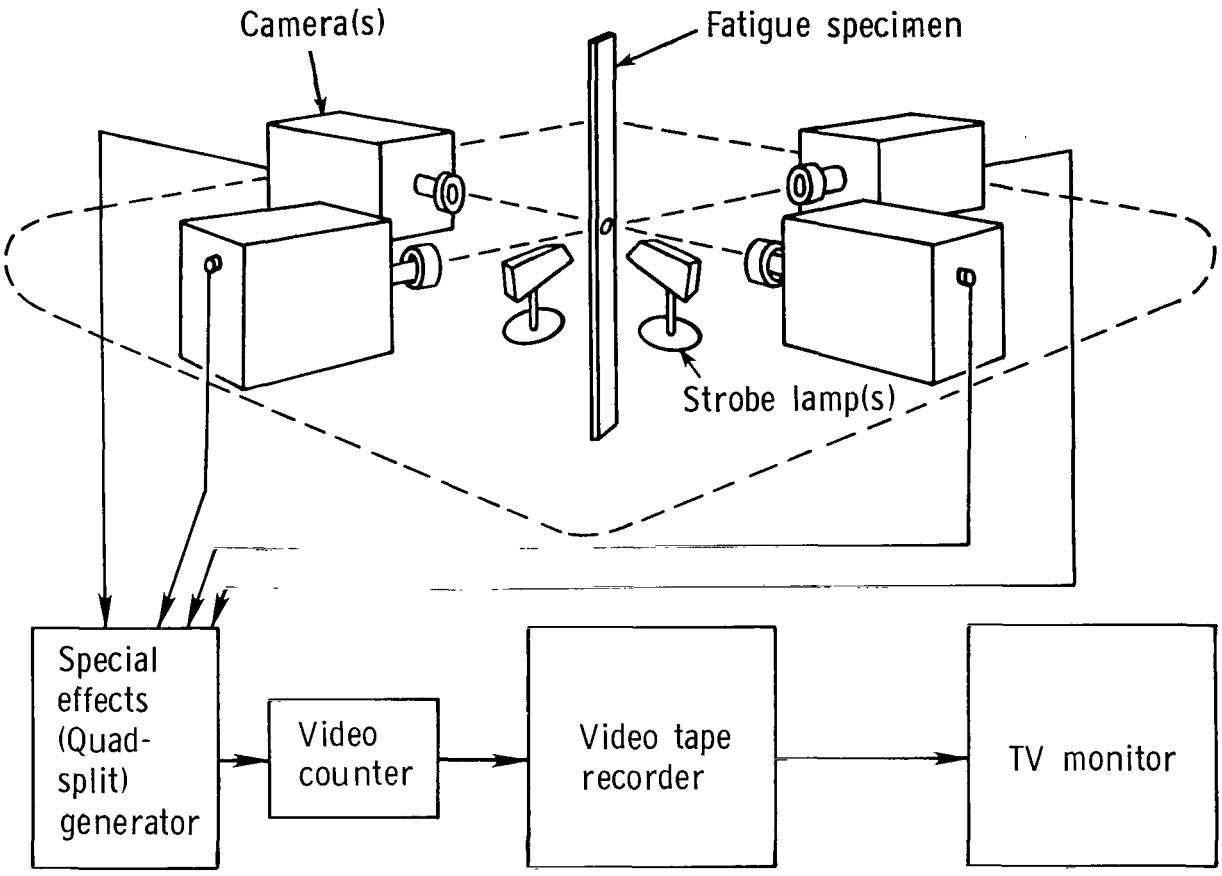

Figure 2.- Diagram of four-camera crack monitoring system.

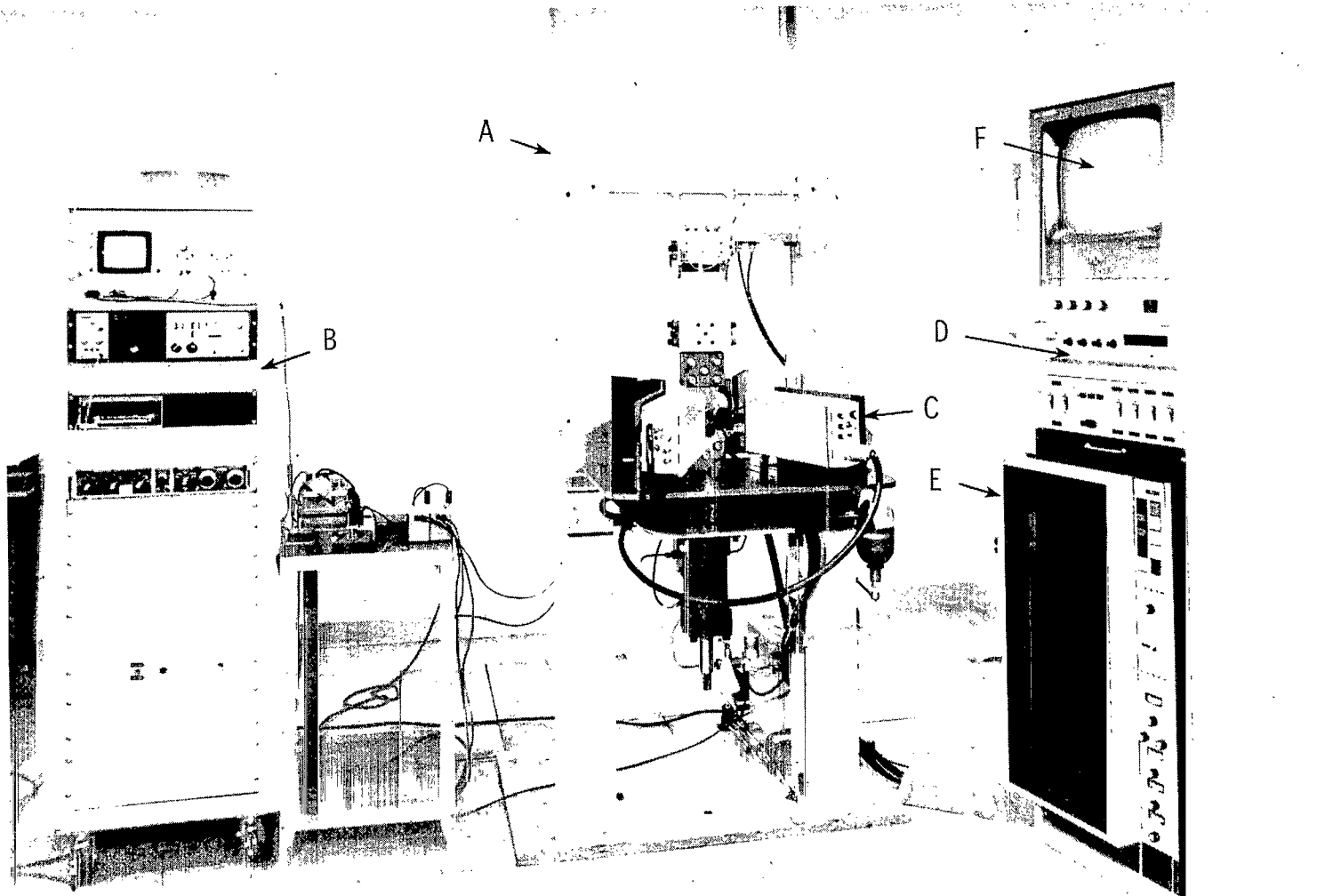

A Testing machine
B Control electronics
C Cameras
D Special effects generator and video counter
E Video tape recorder
F Television monitor

L-75-8202.1

Figure 3.- Overall view of video tape system installed at testing machine.

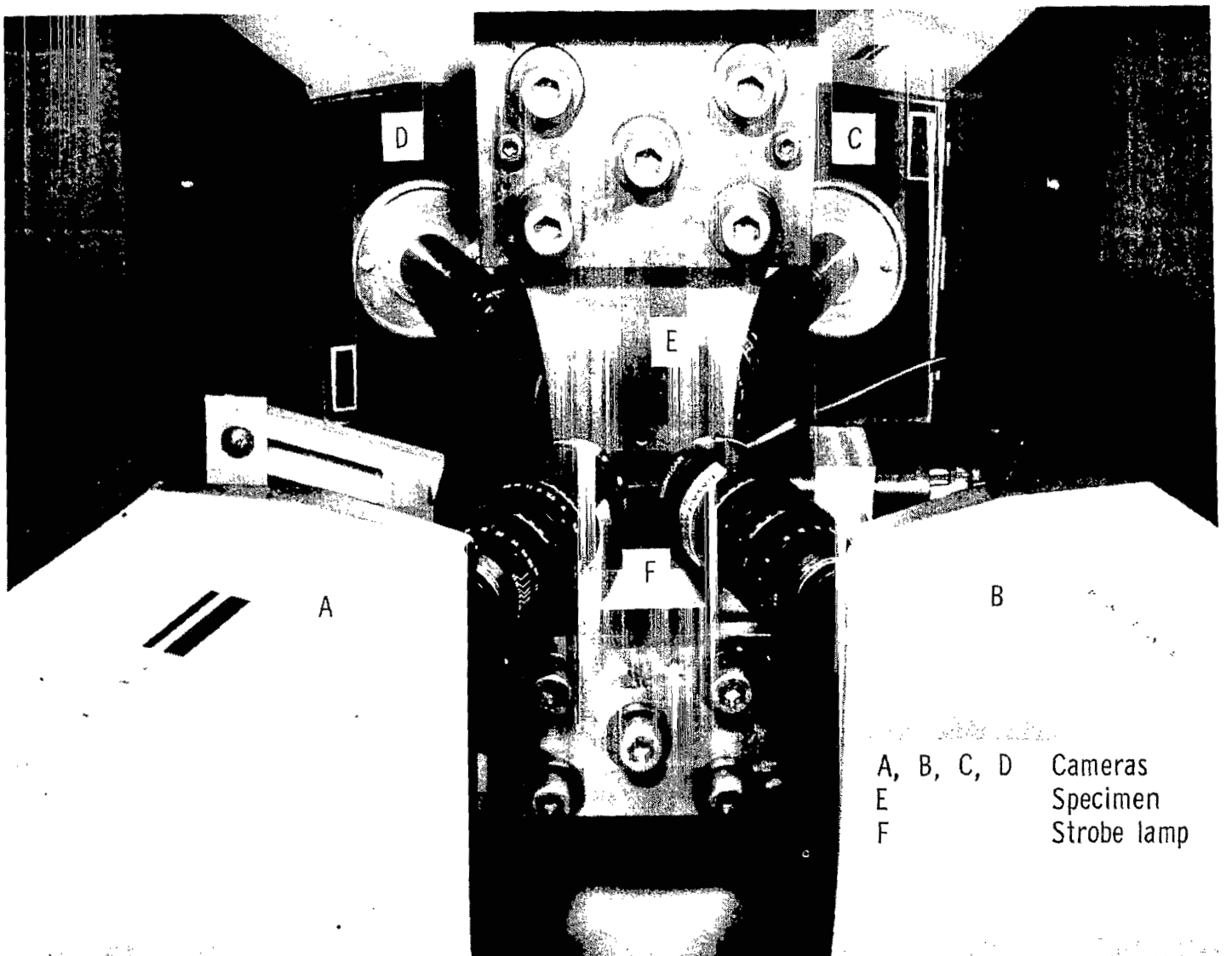

Figure 4.- Closeup view of cameras viewing crack-initiation sites.

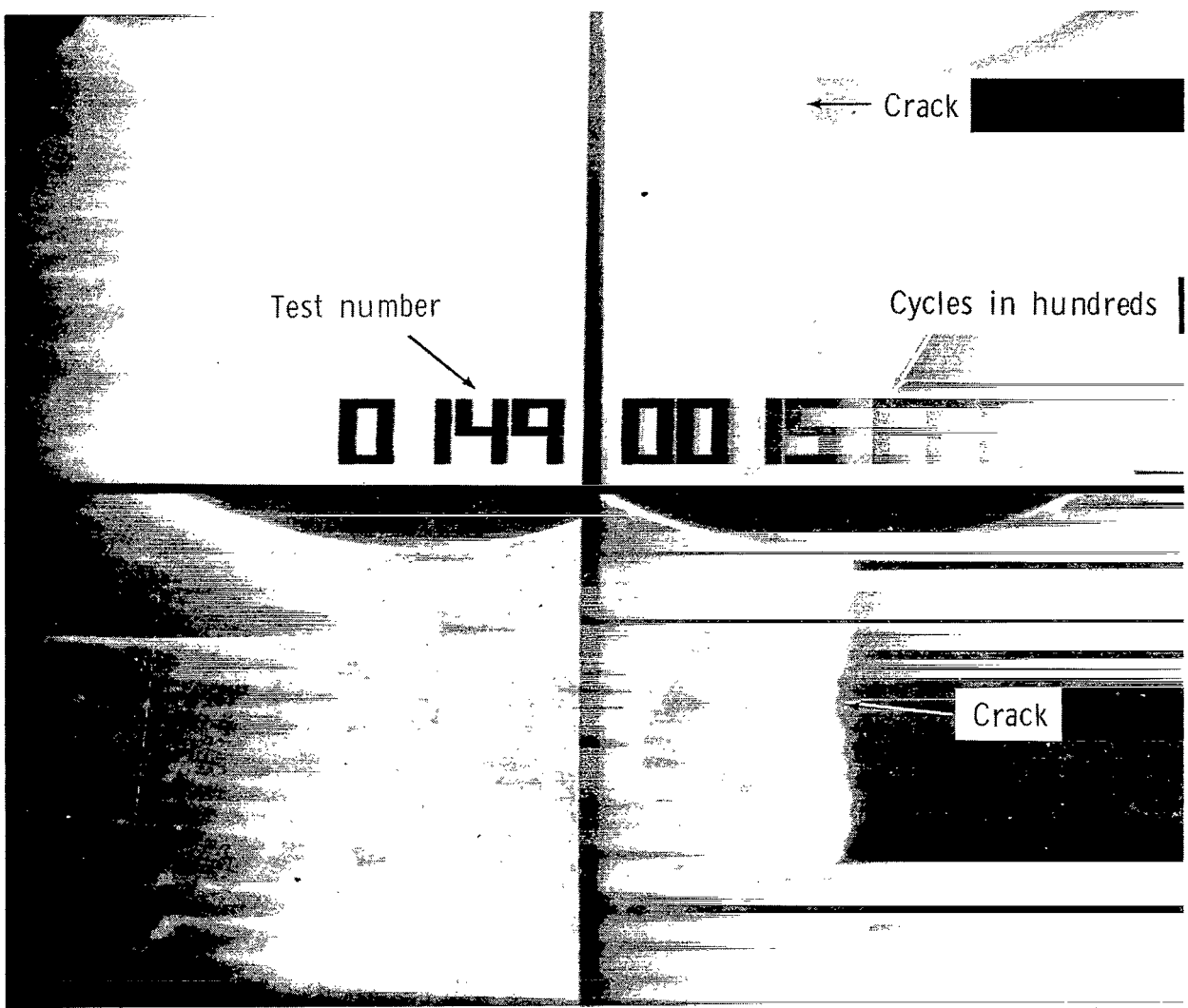

Figure 5.- View of fatigue cracks as they appeared on monitor.

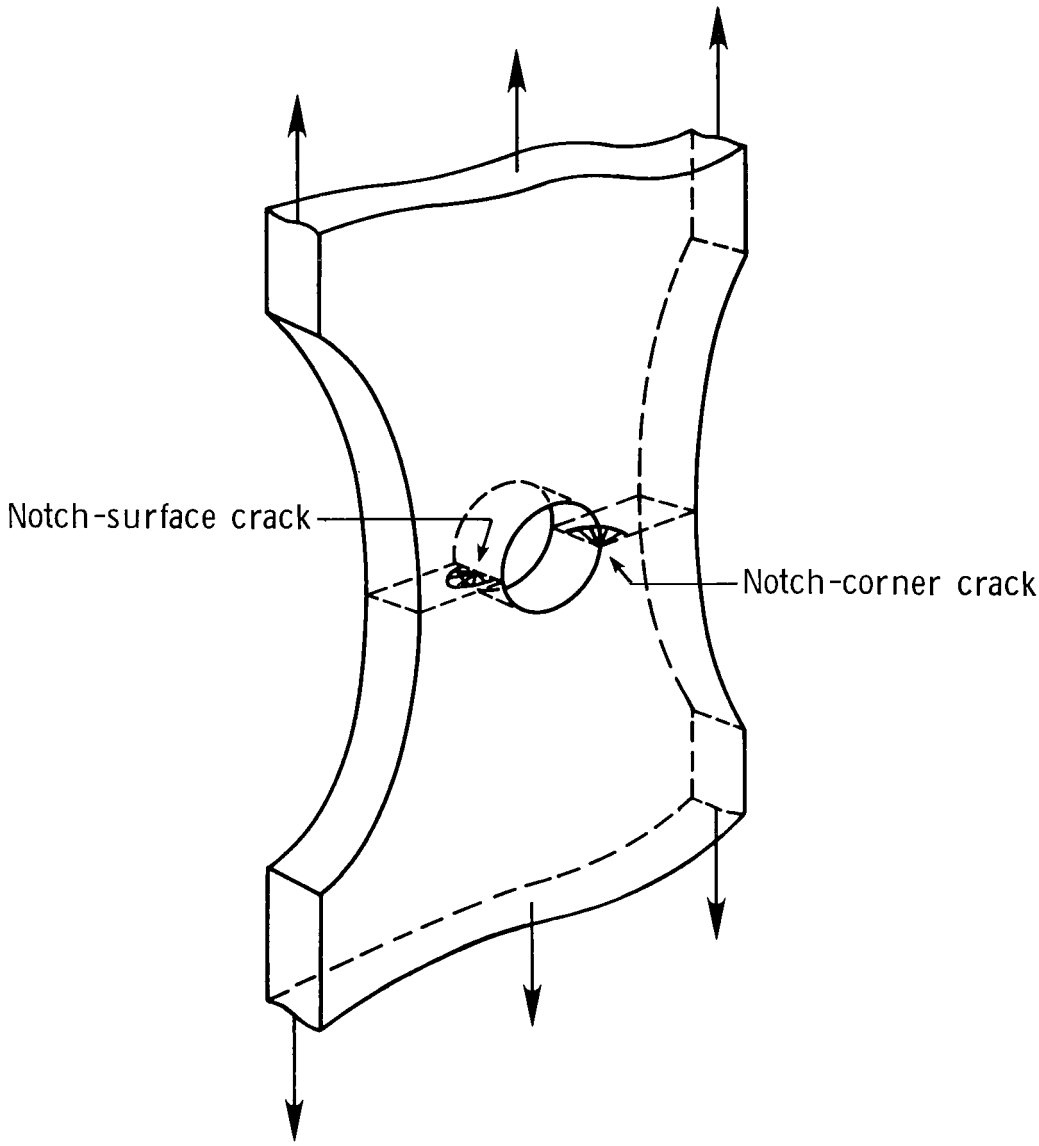

Figure 6.- Crack initiation at notch.

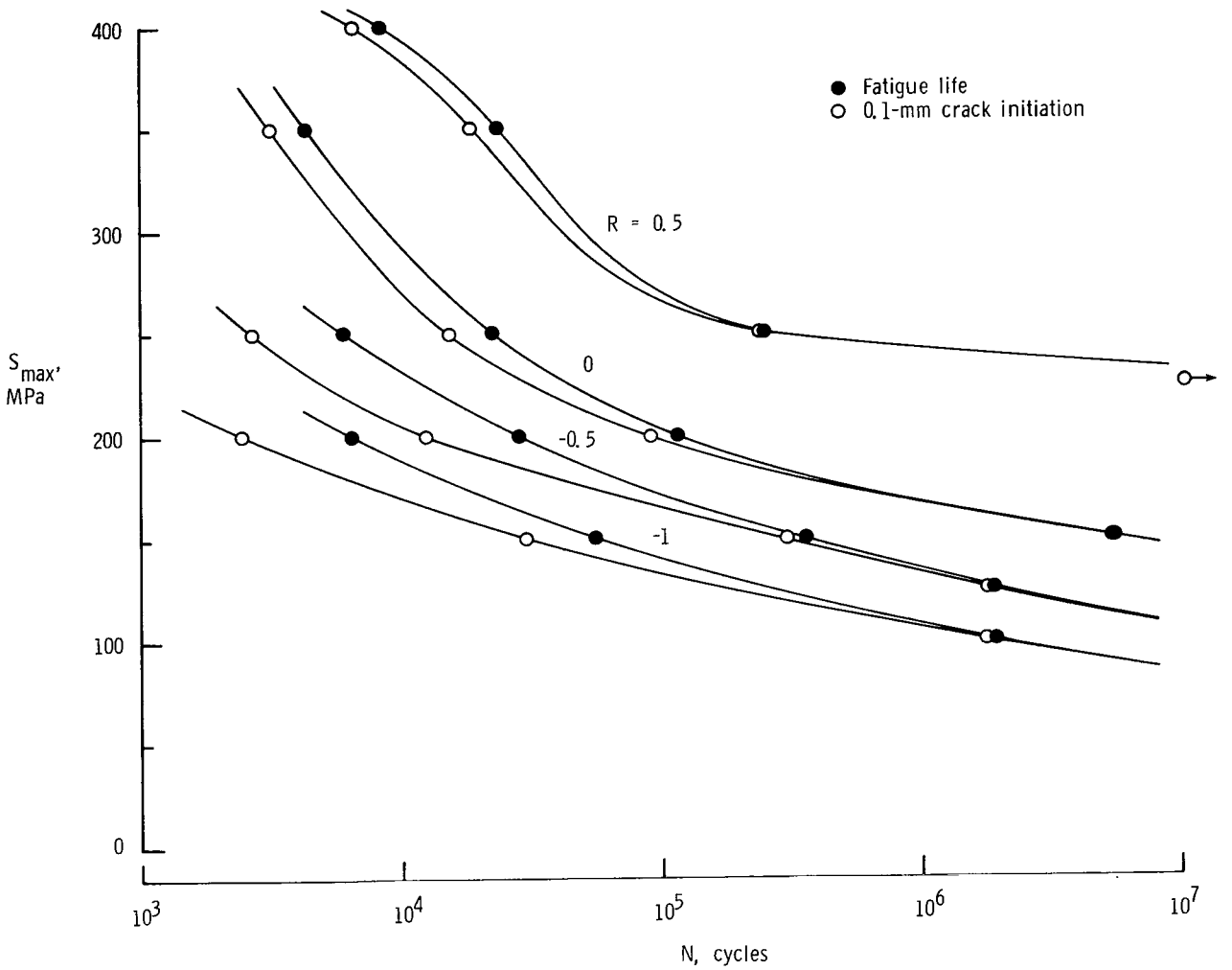

Figure 7.- Corner-crack initiation and fatigue life curves for 2024-T3 notched specimens.

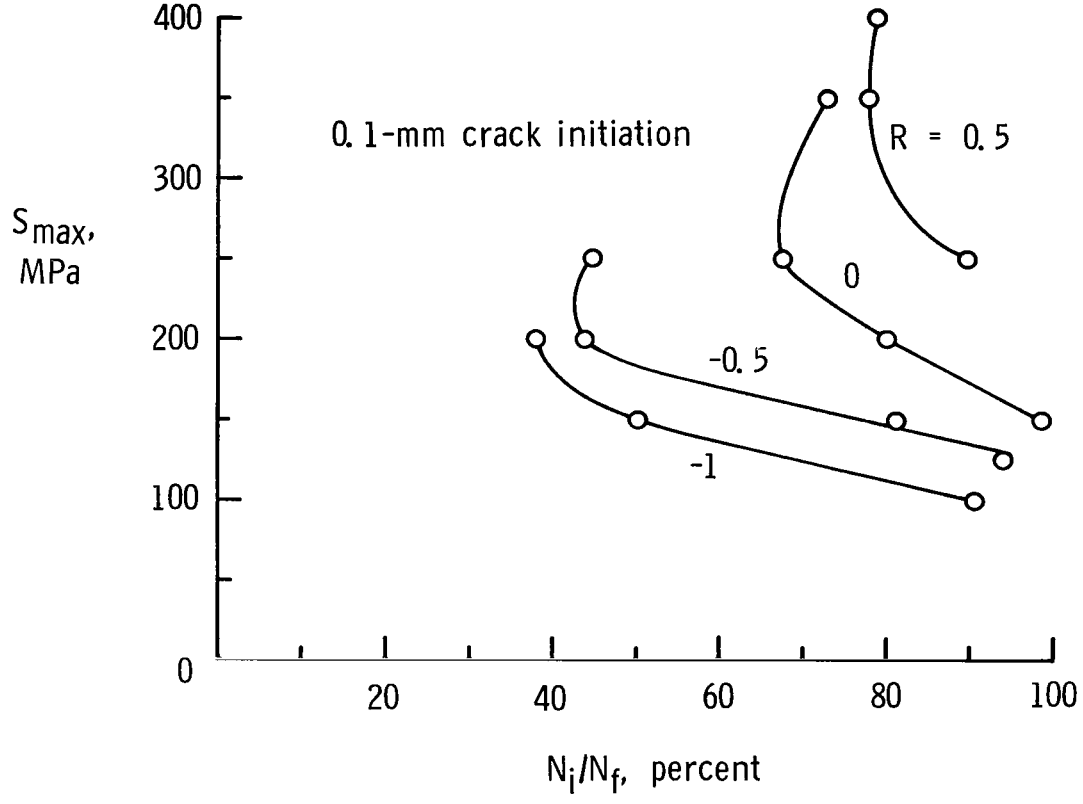

Figure 8.- Percentages of fatigue life covered by notch-corner crack initiation.

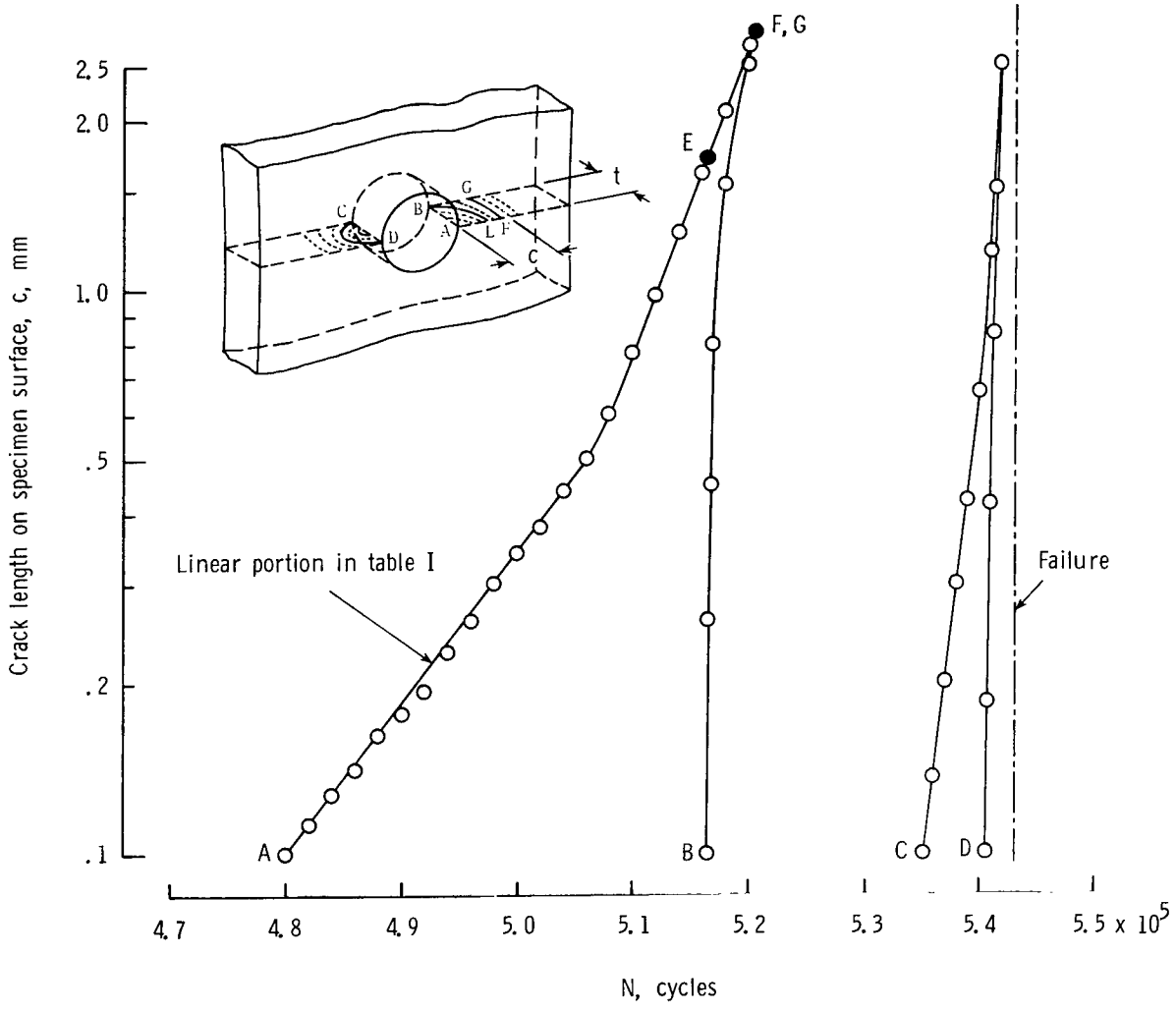

Figure 9.- Typical record of early crack growth on specimen surface. R = -0.5; S_{max} = 150 MPa.

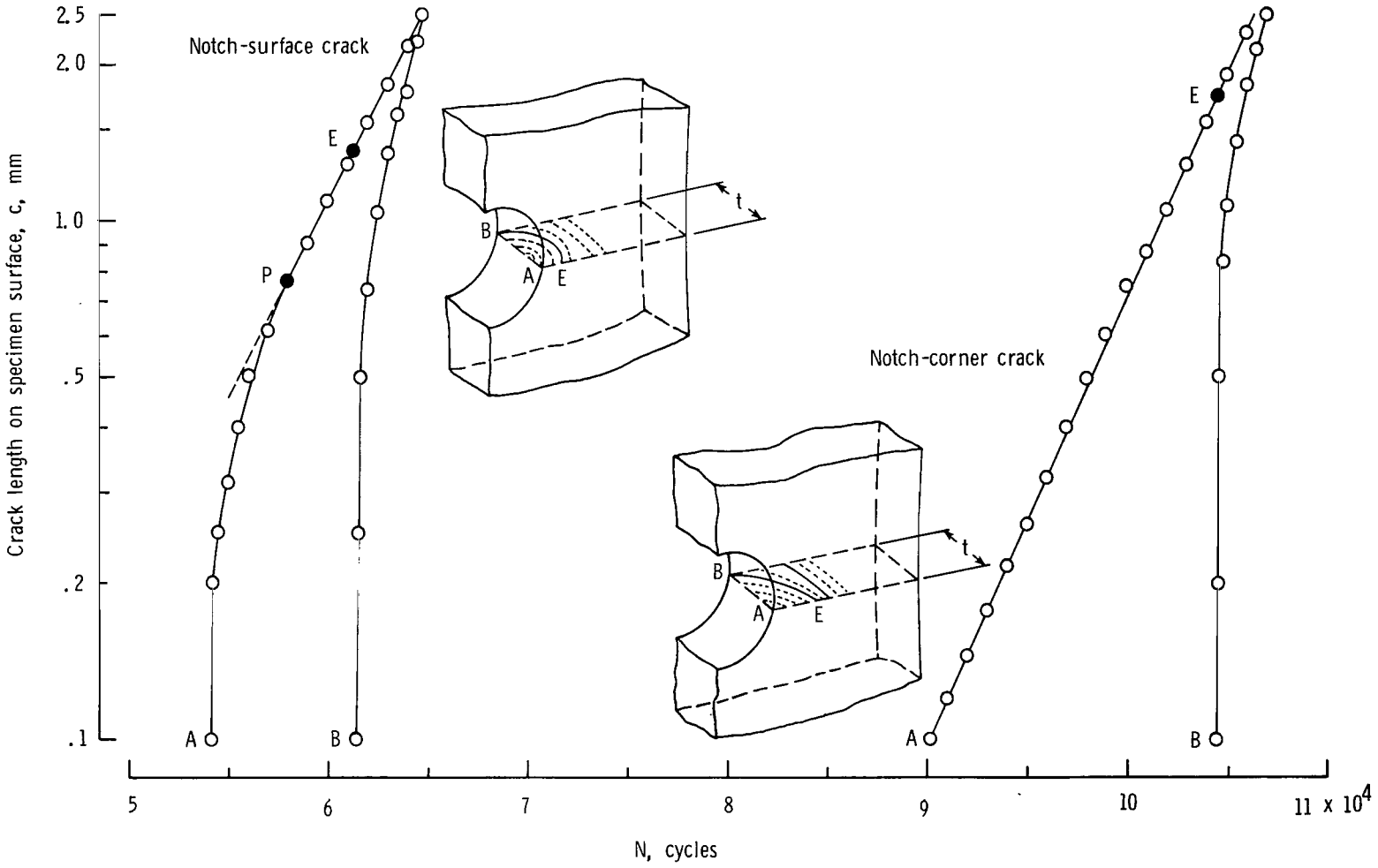

Figure 10.- Typical record of early crack growths for notch-corner and notch-surface cracks. $R = 0$; $S_{max} = 200$ MPa.

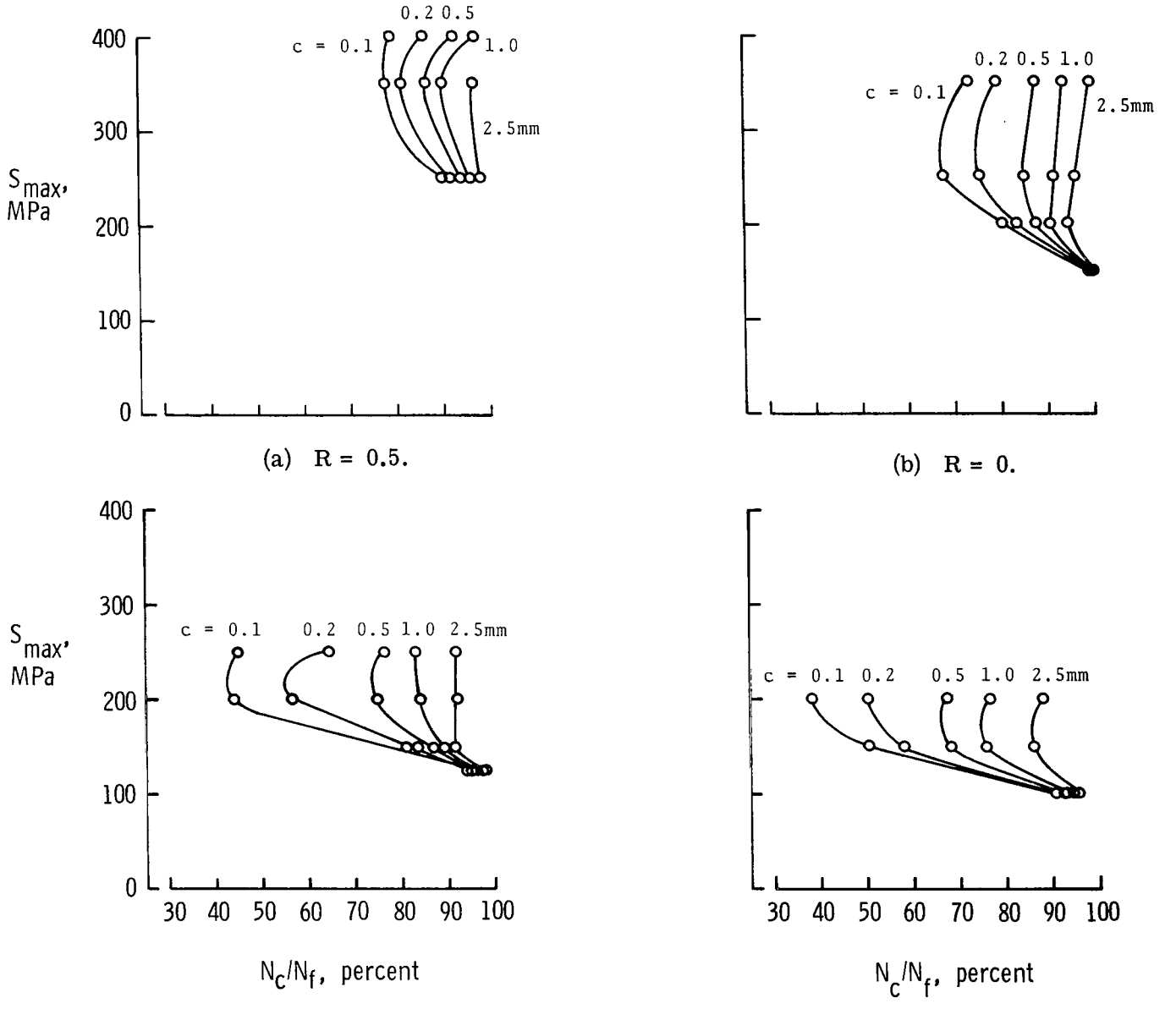

Figure 11.- Percentages of fatigue life required to grow cracks to various lengths.

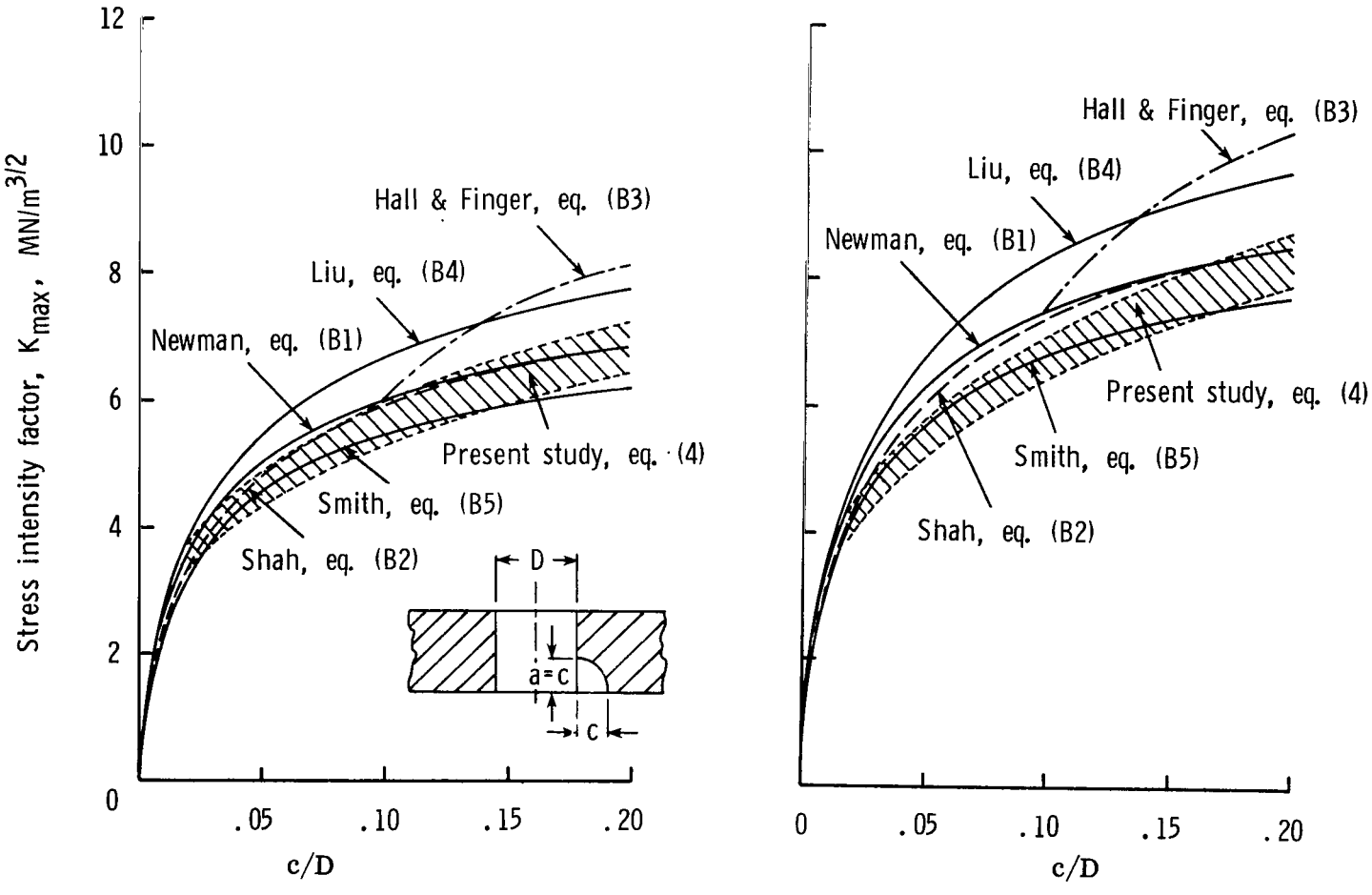

(a) S_{max} = 100 MPa, R = -1.

(b) S_{max} = 125 MPa, R = -0.5.

Figure 12.- Comparison of experimental and analytical stress intensity factors.

"The aeronautical and space activities of the United States shall be conducted so as to contribute . . . to the expansion of human knowledge of phenomena in the atmosphere and space. The Administration shall provide for the widest practicable and appropriate dissemination of information concerning its activities and the results thereof."

—NATIONAL AERONAUTICS AND SPACE ACT OF 1958

NASA SCIENTIFIC AND TECHNICAL PUBLICATIONS

TECHNICAL REPORTS: Scientific and technical information considered important, complete, and a lasting contribution to existing knowledge.

TECHNICAL NOTES: Information less broad in scope but nevertheless of importance as a contribution to existing knowledge.

TECHNICAL MEMORANDUMS: Information receiving limited distribution because of preliminary data, security classification, or other reasons. Also includes conference proceedings with either limited or unlimited distribution.

CONTRACTOR REPORTS: Scientific and technical information generated under a NASA contract or grant and considered an important contribution to existing knowledge.

TECHNICAL TRANSLATIONS: Information published in a foreign language considered to merit NASA distribution in English.

SPECIAL PUBLICATIONS: Information derived from or of value to NASA activities. Publications include final reports of major projects, monographs, data compilations, handbooks, sourcebooks, and special bibliographies.

TECHNOLOGY UTILIZATION PUBLICATIONS: Information on technology used by NASA that may be of particular interest in commercial and other non-aerospace applications. Publications include Tech Briefs, Technology Utilization Reports and Technology Surveys.

Details on the availability of these publications may be obtained from:

SCIENTIFIC AND TECHNICAL INFORMATION OFFICE

NATIONAL AERONAUTICS AND SPACE ADMINISTRATION

Washington, D.C. 20546